Since January 2020 Elsevier has created a COVID-19 resource centre with free information in English and Mandarin on the novel coronavirus COVID-19. The COVID-19 resource centre is hosted on Elsevier Connect, the company's public news and information website.

Bioorganic Chemistry 124 (2022) 105799

Contents lists available at ScienceDirect

Bioorganic Chemistry

journal homepage: www.elsevier.com/locate/bioorg

Hydroxamate and thiosemicarbazone: Two highly promising scaffolds for the development of SARS-CoV-2 antivirals

Yin-Sui Xu [a], Jia-Zhu Chigan [a], Jia-Qi Li [a], Huan-Huan Ding [a], Le-Yun Sun [a], Lu Liu [a], Zhenxin Hu [b], Ke-Wu Yang [a,*]

[a] Key Laboratory of Synthetic and Natural Functional Molecule of the Ministry of Education, College of Chemistry and Materials Science, Northwest University, Xi'an 710127, PR China

[b] Suzhou Genevide Biotechnology Co., Ltd, Suzhou 215123, PR China

ARTICLE INFO

Keywords:
SARS-CoV-2
Main protease
Hydroxamates
Thiosemicarbazones
Inhibitor

ABSTRACT

The emerging COVID-19 pandemic generated by Severe Acute Respiratory Syndrome Coronavirus 2 (SARS-CoV-2) has severely threatened human health. The main protease (M^{pro}) of SARS-CoV-2 is promising target for antiviral drugs, which plays a vital role for viral duplication. Development of the inhibitor against M^{pro} is an ideal strategy to combat COVID-19. In this work, twenty-three hydroxamates **1a-i** and thiosemicarbazones **2a-n** were identified by FRET screening to be the potent inhibitors of M^{pro}, which exhibited more than 94% (except **1c**) and more than 69% inhibition, and an IC_{50} value in the range of 0.12–31.51 and 2.43–34.22 μM, respectively. **1a** and **2b** were found to be the most effective inhibitors in the hydroxamates and thiosemicarbazones, with an IC_{50} of 0.12 and 2.43 μM, respectively. Enzyme kinetics, jump dilution and thermal shift assays revealed that **2b** is a competitive inhibitor of M^{pro}, while **1a** is a time-dependently inhibitor; **2b** reversibly but **1a** irreversibly bound to the target; the binding of **2b** increased but **1a** decreased stability of the target, and DTT assays indicate that **1a** is the promiscuous cysteine protease inhibitor. Cytotoxicity assays showed that **1a** has low, but **2b** has certain cytotoxicity on the mouse fibroblast cells (L929). Docking studies revealed that the benzyloxycarbonyl carbon of **1a** formed thioester with Cys145, while the phenolic hydroxyl oxygen of **2b** formed H-bonds with Cys145 and Asn142. This work provided two promising scaffolds for the development of M^{pro} inhibitors to combat COVID-19.

1. Introduction

The coronavirus disease (COVID-19) generated by Severe Acute Respiratory Syndrome Coronavirus 2 (SARS-CoV-2) has spread widely and rapidly around the globe since it was found in December 2019 [1]. So far, millions of people have died because of the infection of COVID-19 [2]. Though some vaccines have been developed and widely vaccinated, the problems of this viral disease have not been essentially solved, especially now, the emergence of coronavirus variants such as delta and kappa [3–6]. Studies have found that the sera of individuals receiving a dose of Pfizer or AstraZeneca vaccine have limited inhibition of variant Delta [7]. Therefore, there is an urgent need to develop more effective antivirals.

SARS-CoV-2 is a positive-sense and single-stranded RNA virus belonging to the genus betacoronavirus and shares 96% sequence to a bat coronavirus [8]. The virus occupies roughly 26–32 kb in length and encodes some structural, non-structural and accessory proteins. The cleavage of pp1a and pp1ab polyproteins into a single non-structural protein is an essential process in virus replication, and the main protease (M^{pro}) plays a vital role in this process [9–11]. Also, there is no homology between M^{pro} and human protease [12]. Therefore, the M^{pro} is regarded as an important target for designing drugs to combat COVID-19 [13].

The M^{pro}, a nucleophilic cysteine protease, has three domains: I (residues 8–101), II (102–184), and III (201–306). The first two domains are responsible for the structure of protein and the last domain is in charge of the catalytic process [14]. In the active site, Cys145 and His41 form a catalytic binary. The thiol (-SH) group of cysteine is responsible for the hydrolysis and His41 provides the optimal pH conditions to activate the -SH group, thus it achieves a nucleophilic attack on the substrate [15].

So far, many types of M^{pro} inhibitors have been reported, such as peptides, non-peptides, drug molecules and natural products [13,16–18]. Recently, Wang and his colleagues discovered that

* Corresponding author.
E-mail address: kwyang@nwu.edu.cn (K.-W. Yang).

https://doi.org/10.1016/j.bioorg.2022.105799
Received 18 January 2022; Received in revised form 31 March 2022; Accepted 7 April 2022
Available online 18 April 2022

peptidomimetic molecules (boceprevir, GC-376, and calpain inhibitors II and XII) have an IC_{50} value range from single-digit to sub-micromolar [19]. Masitinib, a specific kinase inhibitor, was identified to be effective on tested coronavirus variants (B.1.1.7 and

B.1.351) in vitro [20]. More importantly, recently, Pfizer has released an inhibitor (PF-07321332), currently in Phase 3 clinical trials, is expected to be the first M^{pro} drug to treat

SARS-CoV-2 [21,22]. Although it is early to determine potential inhibitors that would be very effective against the virus, they provide an encouraging start for further coronavirus therapeutics. Both New Delhi metallo-β-lactamase-1 (NDM-1) and M^{pro} are the cysteine proteases [23,24]. As the NDM-1 inhibitors, the Ebsulfur and Ebselen were reported to inhibit M^{pro} [25]. Recently, both hydroxamates and thiosmicarbazones were synthesized in our lab and characterized by NMR and mass spectrometry and evaluated to have inhibitory efficacy on NDM-1 [26,27]. In the same case, we expected these two classes of compounds to have inhibitory activity on M^{pro}, therefore evaluated them. In this work, we focus on screening the M^{pro} inhibitor by fluorescence resonance energy transfer (FRET) method [28,29]. The hydroxamates and thiosemicarbazones were found to be the potential scaffolds to target M^{pro}. Subsequently, the action mechanism of these molecules was characterized and analyzed by enzyme kinetics, jump dilution and thermal shift assays.

2. Results and discussion

2.1. Screening of M^{pro} inhibitor

The SARS-CoV-2 M^{pro} was expressed and purified by the method reported previously [29]. The M^{pro} gene was inserted into the vector PGEX-6P-1 and expressed in BL21 *E. coli*. The protein was purified by Ni-NTA and HiTrap Q FF columns, respectively. The SDS-PAGE of the purified protein is shown in Fig. 1a.

The enzyme activity was assayed by measuring K_m and V_{max} values as previously reported method [30]. The employed fluorescent substrate in this experiment was Mca–AVLQSGFRK(Dnp)K.. Various concentrations of the fluorescent substrate (1–100 μM) were premixed with M^{pro} sample (0.2 μM), respectively. The hydrolysis velocity of substrate was measured, and the data obtained were fitted to the Michaelis-Menten equation to give K_m and V_{max} values. The calculated K_m and V_{max} are 5.4 ± 4.13 μM and 0.68 ± 0.08 nM/s, respectively (Fig. 1b), and K_{cat}/K_m is 6296 M^{-1} s^{-1}, which is consistent with the data (6925 M^{-1} s^{-1}) previously reported [30].

The FRET experiments were performed to screen the potential M^{pro} inhibitors [28,29]. The hydroxamates and thiosemicarbazones were prepared in our lab, characterized by ^1H and ^{13}C NMR, confirmed by HRMS, and reported to be the inhibitors of metallo-β-lactamases [26,27] (Fig. 2). To explore these molecules whether have potential inhibitory effects against M^{pro}. We firstly determined the percent inhibition of these compounds as previously reported method [31]. The hydroxamates **1a-i** and thiosemicarbazones **2a-n** were dissolved in a certain amount of DMSO, and then diluted with assay buffer (20 mM Tris, pH 6.5, 0.4 mM EDTA, 20% glycerol, 120 mM NaCl) [29]. It should be noted that the final concentration of DMSO was less than 0.5%, because the control experiments proved that DMSO at this concentration has no effect on enzyme activity. Percent inhibition of the tested compounds on M^{pro} is shown in Fig. 3. It is clearly to be observed that all hydroxamates (50 μM) exhibited more than 94% inhibition on M^{pro} (except **1c**), and all thiosemicarbazones at same concentration shown more than 69% inhibition. Significantly, the thiosemicarbazones tested had better percent inhibition on M^{pro} than the thiosemicarbazone complexes with iron (III) recently reported (30.62% at 100 μM) [32].

2.2. Determination of IC_{50}

The inhibitor concentrations causing 50% decrease of enzyme activity (IC_{50}) of hydroxamates and thiosemicarbazones on M^{pro} were measured as previously reported method [33]. The concentration range of inhibitors was from 0 to 80 μM, and the substrate and protease concentrations were 20 and 0.2 μM, respectively. The measured IC_{50} data are listed in Table. 1. The collected data show that all of these compounds exhibited potential inhibition against M^{pro}, with an IC_{50} value in the range of 0.12–34.22 μM. The hydroxamates and thiosemicarbazones had an IC_{50} value range of 0.12–31.51 and 2.43–34.22 μM, respectively, **1a** (IC_{50} = 0.12 μM) and **2b** (IC_{50} = 2.43 μM) were found to be the most effective inhibitors in the two classes of compounds, respectively. These assays revealed that both hydroxamates and thiosemicarbazones are attractive scaffolds for the development of M^{pro} inhibitors.

2.3. Inhibition mode assay

Given the best potency, the time-dependent inhibition of hydroxamate **1a** on M^{pro} was assayed. As shown in Fig. 4a, the residual activity of M^{pro} decreased with the increase of premix time of protease with inhibitor (1.25 μM), and **1a** exhibited about 90% inhibition after incubation for 100 min, indicating that **1a** is a time-dependent inhibitor [34].

The reversibility of hydroxamate **1a** and thiosemicarbazone **2b** binding to M^{pro} was evaluated by jump dilution tests [29,35,36]. The M^{pro} sample was incubated with a high concentration of inhibitors

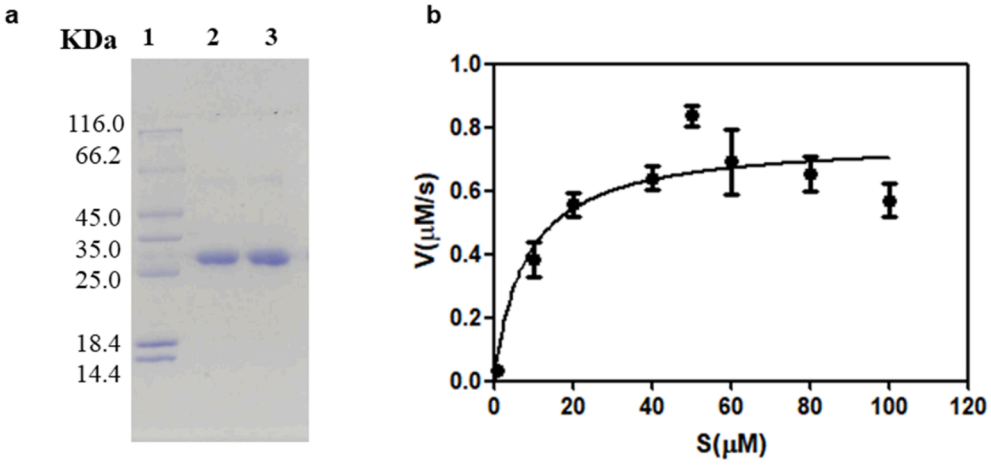

Fig. 1. The SDS-PAGE of the purified SARS-CoV-2 M^{pro} (**a**). Lane 1: protein molecular weight marker, lane 2: purified M^{pro}, lane 3: M^{pro} before cleavage with HRV 3C-protease. Activity of M^{pro} was confirmed by quantification crack of the fluorescent decapeptide Mca–AVLQSGFRK(Dnp)K as substrate (**b**).

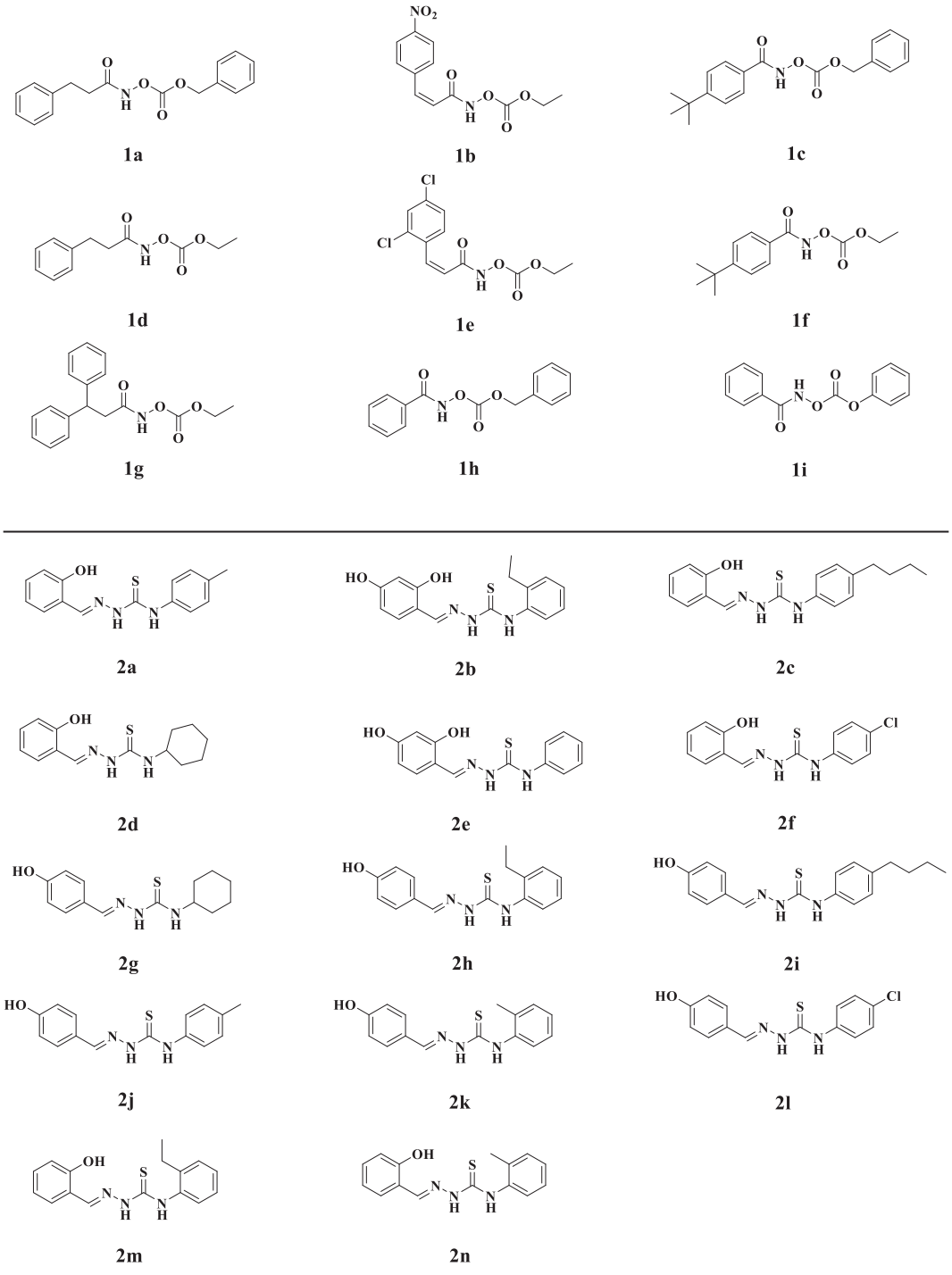

Fig. 2. Structures of the tested hydroxamates (above) and thiosemicarbazones (below) against SARS-CoV-2 M^{pro}.

(equivalent to 50 × IC_{50}) **1a** (6 μM) and **2b** (122 μM) for 2 h, respectively, so that the inhibitor could fully occupy enzymatic active sites, the resulting mixtures were diluted 100-fold with the fluorescence substrate solution, and the enzymatic residual activity was determined by monitoring the fluorescence. It is clearly observed in Fig. 4b that in the presence of **1a**, the enzyme activity did not recover after the dilution. However, the enzyme treated with **2b** recovered about 60% activity after dilution for 4000 s. These results indicate that the thiosemicarbazone reversibly, but hydroxamate like the Ebselen and Ebsulfur, irreversibly inhibit M^{pro} [29].

To further study the inhibition mode of the hydroxamates and thiosemicarbazones on M^{pro}, **1a** and **2b** were chosen to determine the enzyme kinetic parameters [37–39]. The above assay reveals that **1a** inhibit M^{pro} in a time-dependent pattern, and the kinetic progression curves exhibited a biphasic character (Fig. 5a), suggesting the inactivation rate follows pseudo-first-order rate kinetics. These results imply that the hydroxamate may covalently bind to the target [38]. The K_{obs} (observed rate constant) were fitted against inhibitor concentration by nonlinear regression to calculate K_I (the concentration of inacti-vator at the half-maximum inactivation rate constant), k_{inact}, and k_{inact} /K_I values, which are 1.18 ± 0.43 μM, 0.0075 ± 0.0005 s^{-1}, and 6.4 × 10^3 $M^{-1}s^{-1}$, respectively [37].

The inhibition mode of thiosemicarbazone **2b** was identified by analyzing Lineweaver–Burk plots, and K_i (inhibiton constant) value was

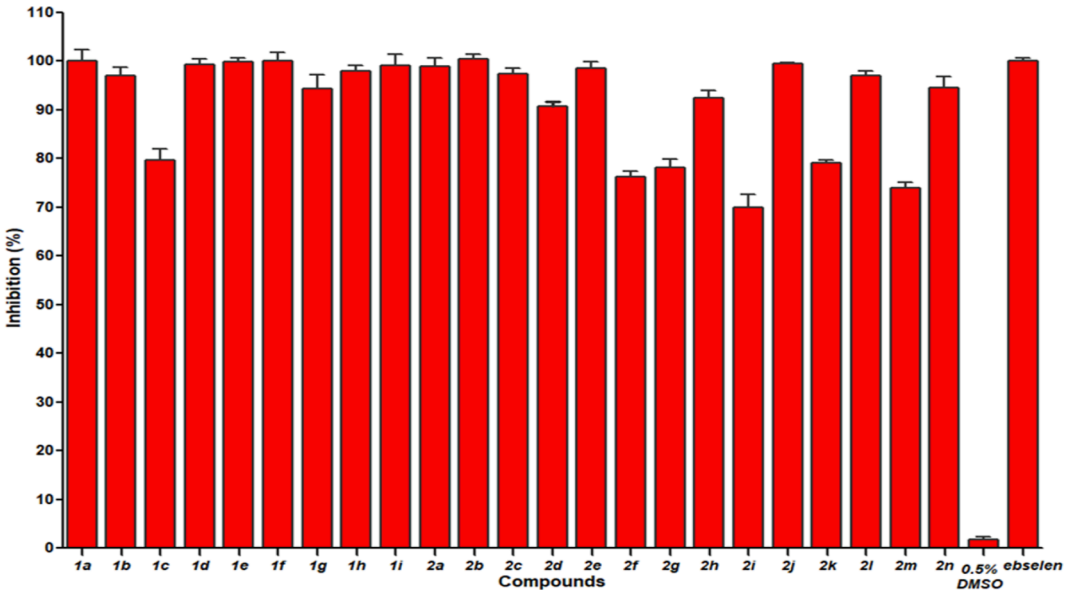

Fig. 3. Percent inhibition of hydroxamates **1a-i** and thiosemicarbazones **2a-n** (50 μM) against M^{pro}. 0.5% DMSO was used as negative control and ebselen was used as positive control.

Table 1
The inhibitory activities (IC_{50}, μM) of hydroxamates and thiosemicarbazones on $M^{pro.}$

Compd.	IC_{50}	Compd.	IC_{50}	Compd.	IC_{50}	Compd.	IC_{50}
1a	0.12	**1 g**	18.78	**2d**	17.61	**2j**	3.25
1b	4.3	**1 h**	11.7	**2e**	8.45	**2 k**	28.81
1c	31.51	**1i**	3.6	**2f**	32.94	**2 l**	9.11
1d	0.15	**2a**	3.61	**2 g**	32.33	**2 *m***	33.40
1e	0.42	**2b**	2.43	**2 h**	19.10	**2*n***	20.74
1f	1.46	**2c**	4.37	**2i**	34.22		

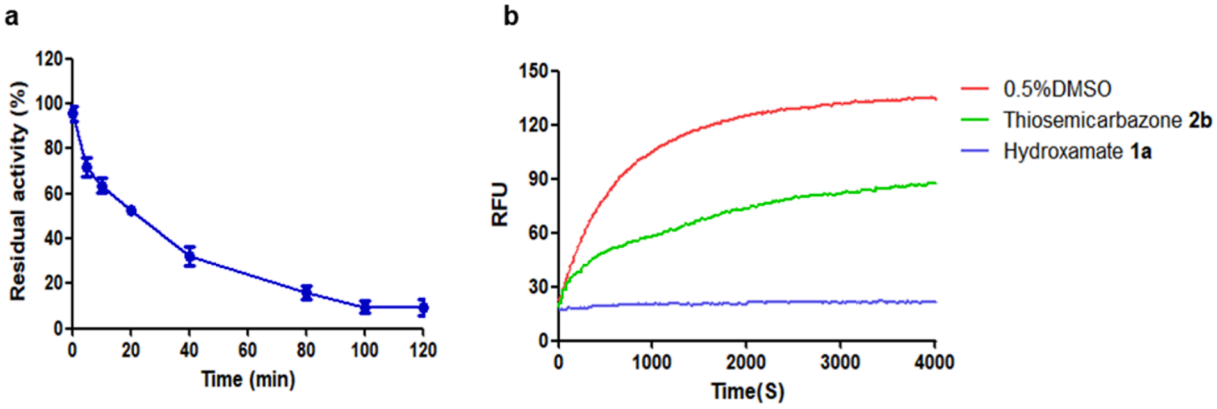

Fig. 4. Time-dependent inhibition curve of hydroxamate **1a** (1.25 μM) on M^{pro} (**a**). Progress curves of M^{pro} activity change in the presence of hydroxamate **1a** and thiosemicarbazone **2b** (**b**). 0.5% DMSO was used for the blank control.

determined by fitting initial velocity versus substrate concentrations at each inhibitor concentration using SigmaPlot 12.0. The concentrations of substrate and inhibitor were in the range of 2.5–20 and 0–10 μM, respectively. The enzyme (0.2 μM) was incubated with inhibitor for 2 h, and the reaction was monitored when substrate was added. The Lineweaver–Burk plots of fluorescent substrate hydrolysis by M^{pro} in the absence and presence of **2b** are shown in Fig. 5b, which indicate that **2b** is a competitive inhibitor [39], and the calculated K_i value is 3.9 μM.

2.4. Thermal shift assay

Thermal shift analysis, a powerful technique, is used to screen molecules that impact protein stability via monitoring a shift in the melting temperature (T_m) of the protein [40]. In general, the binding of a small molecule stabilizes protein, leading to an increased T_m value. However, a decreased T_m value results in destabilization of the protein [41]. To investigate the interaction of M^{pro} with inhibitors, the M^{pro} (20 μM) was premixed with hydroxamate **1a** (20 μM) and thiosemicarbazones **2b** (20 μM) for 2 h, respectively, and then the mixtures were treated with the SYPROR orange dye. The reaction of the protein and inhibitor was

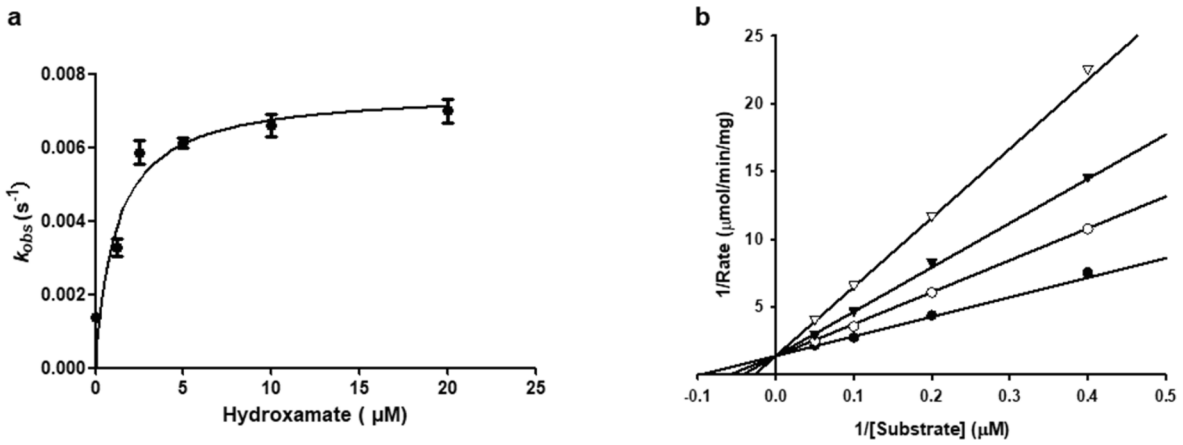

Fig. 5. The hyperbolic plots of K_{obs} against concentrations of hydroxamate **1a** (**a**). The Lineweaver-Burk plots of M^{pro} catalyzed hydrolysis of thiosemicarbazone **2b**. The concentrations of inhibitors were 0 (●), 2.5 (○), 5(▼), 10 (▽) μM (**b**).

heated from 25 to 80 °C in 0.8 °C increment. As shown in Fig. 6a, the T_m of M^{pro} was 54.49 °C. While in the presence of **1a**, the determined T_m value of protein decreased to 50.81 °C, indicating that binding of hydroxamates to protein leads to destabilization, like the M^{pro} inhibitors ebselen and disulfiram previously reported [42]. In contrast, in the presence of **2b**, the T_m of protein increased from 54.49 to 56.11 °C, suggesting that the tightly binding of thiosemicarbazones to M^{pro} increases the stability of the protein.

Moreover, we performed a dose-dependent determination of T_m as the reported method [33]. The M^{pro} (20 μM) was mixed with various concentrations of **1a** and **2b** (10–100 μM) for 2 h, respectively. As shown in Fig. 6c, the melting temperature shifts (ΔT_m) of M^{pro} increased with the increase of inhibitor concentration (10–100 μM), implying that the stabilization of M^{pro} to thermal denaturation is concentration-dependent.

2.5. Dithiothreitol (DTT) assay

To verify the action site of hydroxamates **1a** to M^{pro}, DTT experiments were performed as previously reported method [42]. The M^{pro} (0.2 μM) was premixed with **1a** (1.25 μM) in the assay buffer (see above) supplemented with and without DTT (4 mM) for 2 h, respectively. The fluorescent substrate (20 μM) was added to the mixture solution and then the initial reaction rate was determined. As shown in Fig. 7a, 1a had a potential inhibitory effect on the protein in the absence of DTT. Nevertheless, **4a** did not show a significant inhibition on the protein in the presence of DTT.

Meanwhile, we also carried out a dose-dependent inhibition experiments of M^{pro}. As shown in Fig. 7b, the residual activity of protein decreased with the increase of **1a** concentration (0–10 μM) in the absence of DTT. In contrast, in the presence of DTT, the enzymatic activity was not effectively inhibited. Also the residual activity of enzyme

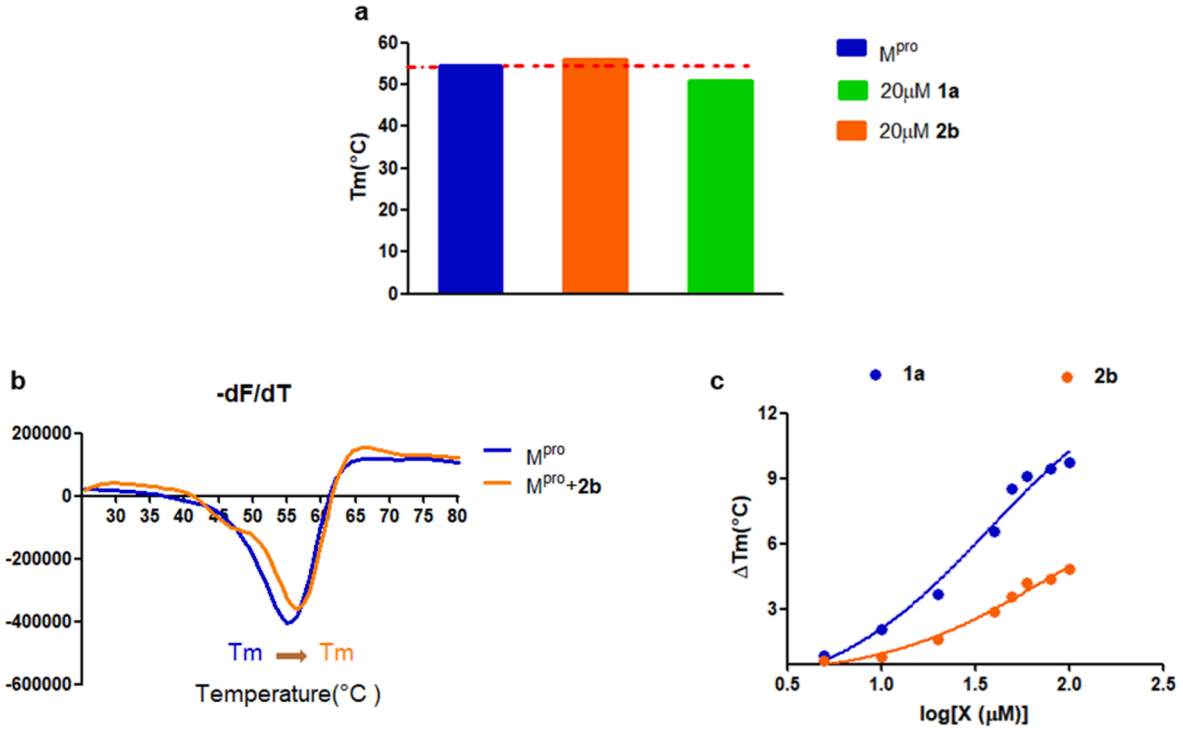

Fig. 6. The melting temperature (T_m) of M^{pro} in the absence and presence of **1a** and **2b (a).** Fluorescence based thermal shift assays of **2b** interaction with M^{pro} as indicated by dF/dT (**b**). Dose-dependent melting temperature shift (**c**).

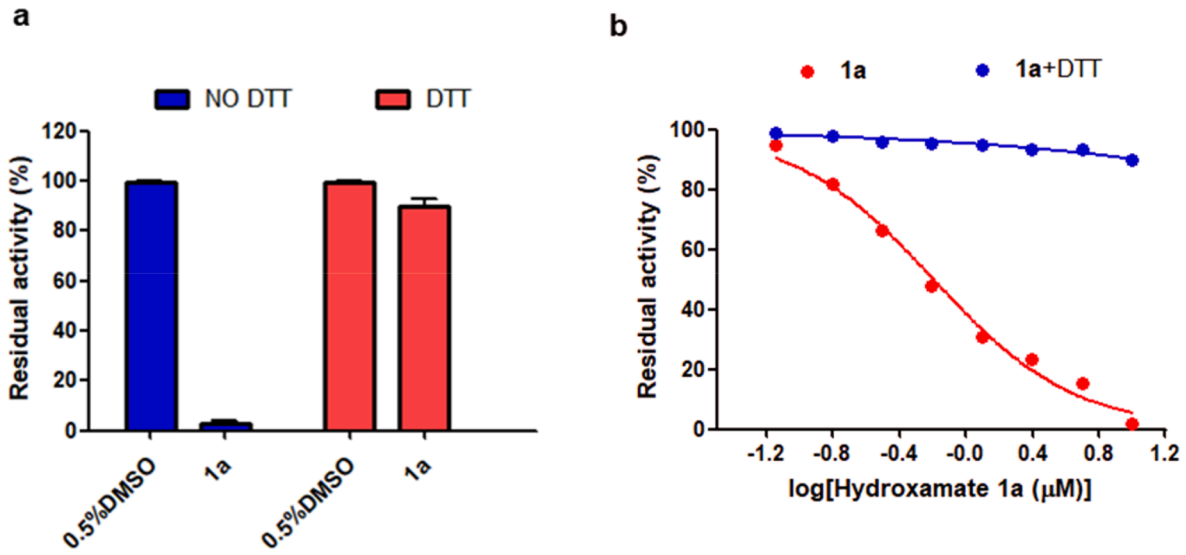

Fig. 7. Inhibition (**a**) and dose-dependent inhibition (**b**) of hydroxamate **1a** on M^{pro} in the presence and absence of DTT.

was not associated with inhibitor concentration. The inhibition of **1a** on the enzyme was abolished, probably because the binding site of **1a** on enzyme was disrupted by DTT. The above experimental results implied that the inhibition of hydroxamate **1a** on M^{pro} was realized by cysteine modification and **1a** is also the promiscuous cysteine protease inhibitor [29].

2.6. Molecular modeling

To predict the binding affinity and pose of both hydroxamates and thiosemicarbazones to M^{pro}, **1a** and **2b** were docked into the active sites of the crystal structure of M^{pro} (PDB ID: 6LU7) [43]. The minimized binding free energy of **1a** and **2b** were calculated to be −4.53 and −6.64 kcal/mol, respectively. Docking studies revealed that the carbonyl and amine group of **1a** first approach Cys145 through H-bond, and **1a** also interacted with His41 residue, increasing the affinity of this substructure to the protein. Subsequently, the action mechanism might be as previously reported [15,19,44–46]. The SH group of Cys145 was deprotonated by His41, initiated a nucleophilic attack on benzyloxycarbonyl carbon to form thioester (Fig. 8a), and control experiments proved that *N*-hydroxy-3, 3-diphenylpropanamide had no inhibitory effect on M^{pro}, which also proved that the interaction site of the hydroxamate and protease is the benzyloxycarbonyl instead of amide carbonyl.

For the complex M^{pro}/**2b** (Fig. 8b), the phenolic hydroxyl oxygen formed H-bond with Cys145 (2.6 Å) and Asn142 (3.0 Å), also two nitrogen atoms of thiourea interacted with Gln166 (2.3 Å, 2.6 Å) through H-bond, tightly anchoring the **2b** complex in the active site of M^{pro} [47].

2.7. Cytotoxicity assay

The potential toxicity of compounds is a vital criterion to evaluate their clinical medical applications. The cytotoxicity of the hydroxamate **1a** and thiosemicarbazone **2b** (1–400 μM) were assayed by using mouse fibroblast (L929) cells [48,49]. As shown in Fig. 9, the cell viability was over 98% in the presence of 25 μM **1a**, but only 80% of cells tested maintained viability in the presence of **2b** at same concentration, indicating that the hydroxamate has low cytotoxicity, and the thiosemicarbazone has certain cytotoxicity on L929 cells.

Given that both thydroxamates and thiosemicarbazones were reported to have anticancer efficacy [50–53], we performed toxicity assay and fluorescence microscopy images of the human breast cancer cells (MCF-7) treated with these compounds (see supporting information) [54,55]. As shown in Fig. S1, more than 98% of cells maintained viability in the presence of **1a** and **2b** (25 μM). However, the cell viability was over 85% for 100 μM inhibitors (Fig.S2) and less than 30% for 800 μM inhibitors, indicating that **1a** and **2b** have low cytotoxicity at a low concentration.

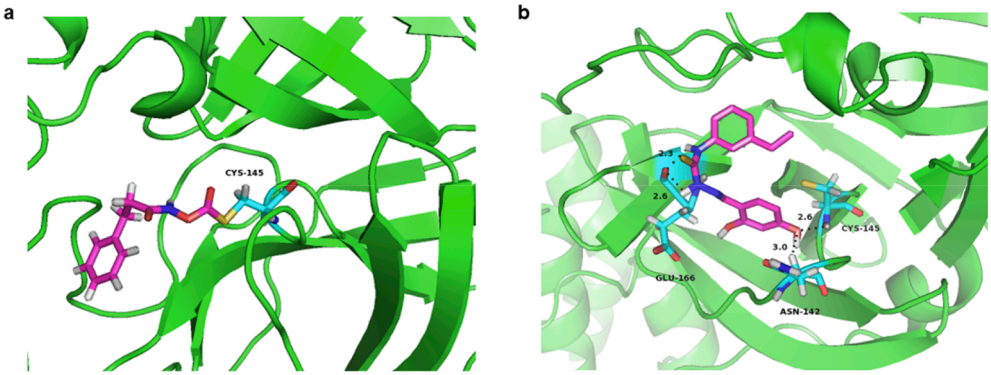

Fig. 8. The lowest-energy conformations of the complex of inhibitors with M^{pro}. Interactions formed between hydroxamate **1a** (**a**) and thiosemicarbazone **2b** (**b**) and surrounding residues, the M^{pro} skeleton is exhibited as a green cartoon and the inhibitors and residues are exhibited as sticks colored by elements (N, blue; O, red; H, white; S, yellow; C, purple). (For interpretation of the references to colour in this figure legend, the reader is referred to the web version of this article.)

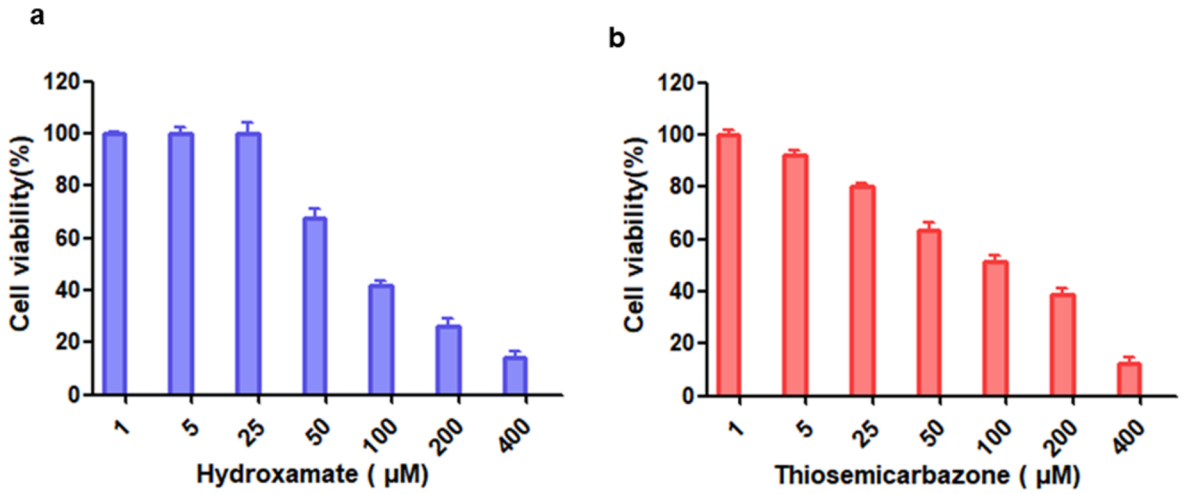

Fig. 9. The cytotoxicity assays of inhibitors (1–400 μM) hydroxamate **1a** (**a**) and thiosemicarbazone **2b** (**b**) on mouse fibroblast (L929) cells.

3. Materials and methods

3.1. Enzymatic activity assay

The enzyme activity was evaluated according to previously described method [30]. The fluorescence substrate Mca–AVLQSGFR-K (Dnp)K was prepared into samples with different concentration (1–100 μM). The M^{pro} (0.2 μM) was added to the assay buffer containing substrate, and then the fluorescence change of substrate was monitored on Microplate Reader (Var ioskan flash, emission, 405 nm / excitation, 320 nm) for 4 min. The initial reaction rate of enzyme hydrolyzing substrate was calculated by linear regression (Graphpad Prism 5) and the Michaelis-Menten equation was used to plot against the substrate concentration.

3.2. Enzymatic inhibition assay

To obtain the percent inhibition, the hydroxamates **1a-i** and thiosemicarbazones **2a-n** were first dissolved in DMSO and then diluted with assay buffer. The protease (0.2 μM) was mixed with inhibitors (50 μM) at 37 °C for 2 h. Finally, the substrate (20 μM) was added to the mixture solutions, and then the hydrolysis of fluorescence substrate was monitored on Microplate Reader for 1 min. The enzyme was treated with 0.5% DMSO as the negative control and ebselen was used as the positive control [31].

3.3. Inhibition mode assays

The inhibition mode of hydroxamate **1a** on M^{pro} was evaluated and the kinetic parameters were determined [37,38]. In detail, the substrate (20 μM) was added into assay buffer supplement with **1a** at different concentrations (1–30 μM), respectively. When the enzyme sample was added and then the hydrolysis of fluorescence substrate was monitored on Microplate Reader for 5 min. The K_{obs} was obtained by fitting the enzyme inhibition progress curves to the equation (1).

$$R_t - R_0 = \frac{V_0}{K_{obs}}\left(1 - e^{-tK}obs\right) \quad (1)$$

Where R_t is the fluorescence value at time t, R_0 is the initial fluorescence value at time 0, V_0 is the initial reaction rate, K_{obs} values was obtained and then fitted into Equation (2) to aqucire k_{inact} and K_I values.

$$K_{obs} = \frac{K_{inact}[I]}{K_I + [I]} \quad (2)$$

Where [I] is inhibitor concentration, k_{inact} is the rate constant of inactivation.

3.4. Thermal shift assay

Thermal shift assay was performed according to the previously described [33,40]. The dyes used in this experiment was SYPRO Orange (10 X final concentration), M^{pro} (20 μM) was premixed with hydroxamate **1a** and thiosemicarbazone **2b** (10–100 μM) in Tris buffer (60 mM, 200 mM NaCl, pH 7.5) for 2 h, respectively. When the SYPRO Orange was added in 96-well plate and then the fluorescence was monitored on an ICycler (Bio-Rad, emission, 570 nm / excitation, 300 nm) from 25 to 80 °C in steps of 0.8 °C. The protein melting temperature (T_m) was obtained by using the Boltzmann model (Protein Thermal Shift Software v1.3) to analyze the mid log of the transition state of protein from the nature to the denatured. The enzyme sample in wells was treated with 0.5% DMSO as blank controls, and both ligands only control and no protein control were used as the negative control to exclude the contamination in wells and ligand–dye interactions interference.

3.5. Cytotoxicity assay

The cytotoxicity of hydroxamate **1a** and thiosemicarbazone **2b** were tested with L929 cells. The cells were cultured into 96-well plates (1.0×10^3 cells /well) containing culture medium for 2 days. Subsequently, the cells were premixed with inhibitors (1–400 μM) for another 24 h, respectively. The cell supernatant was removed and added MTT solution (10 μL/well) for 4 h, and then added DMSO (100 μL/well) for 20 min. The OD_{490} values (optical density) were measured on Microplate Reader [48].

4. Conclusions

The main protease (M^{pro}) that the SARS-CoV-2 viral replication employed was expressed and purified by Ni-NTA and HiTrap Q FF columns, and K_m and V_{max} were determined to be 5.4 ± 4.13 μM and 0.68 ± 0.08 nM/s, respectively. Twenty-three hydroxamates **1a-i** and thiosemicarbazones **2a-n** were identified by FRET screening to be the potent inhibitors of M^{pro}, which exhibited more than 94% (except **1c**) and more than 69% inhibition, and an IC_{50} value in the range of 0.12–31.51 and 2.43–34.22 μM, respectively, the hydroxamate **1a** (IC_{50} = 0.12 μM) and thiosemicarbazone **2b** (IC_{50} = 2.43 μM,) were found to be the most effective inhibitors. The enzyme kinetics, jump dilution and thermal shift assays showed that **2b** is a competitive inhibitor, while **1a** is a time-dependent inhibitor; **2b** reversibly but **1a** irreversibly bound to the target; the binding of **2b** increases but **1a** decreases the stability of the

protein, and DTT assays indicate that **1a** is the promiscuous cysteine protease inhibitor. Cytotoxicity assays showed that **1a** has low cytotoxicity and **2b** has certain cytotoxicity on the mouse fibroblast cells (L929). Docking studies revealed potential binding modes of the two most potent inhibitors to M^{pro}, in which the benzyloxycarbonyl carbon of **1a** might be formed a thioester bond with Cys145, while the phenolic hydroxyl oxygen of **2b** formed H-bonds with Cys145 and Asn142.

Declaration of Competing Interest

The authors declare that they have no known competing financial interests or personal relationships that could have appeared to influence the work reported in this paper.

Acknowledgments

This work was supported by the grant (22077100) from the National Natural Science Foundation of China and the grant (2019KW-068) from Shaanxi Province International Cooperation Project.

Appendix A. Supplementary material

Supplementary data to this article can be found online at https://doi.org/10.1016/j.bioorg.2022.105799.

References

[1] C. Dimeglio, M. Milhes, J.-M. Loubes, N. Ranger, J.-M. Mansuy, P. Trémeaux, N. Jeanne, J. Latour, F. Nicot, C. Donnadieu, J. Izopet, Influence of SARS-CoV-2 variant B.1.1.7, vaccination, and public health measures on the spread of SARS-CoV-2, Viruses 13 (5) (2021) 898.
[2] A. Pascual-Iglesias, J. Canton, A.M. Ortega-Prieto, J.M. Jimenez-Guardeño, J. A. Regla-Nava, An overview of vaccines against SARS-CoV-2 in the COVID-19 pandemic era, Pathogens 10 (8) (2021) 1030.
[3] Q.A. Al Khames Aga, W.H. Alkhaffaf, T.H. Hatem, K.F. Nassir, Y. Batineh, A.T. Dahham, D. Shaban, L.A. Al Khames Aga, M.Y.R. Agha, M. Traqchi, Safety of COVID-19 vaccines, J Med Virol, 93 (2021) 6588-6594.
[4] T. Farinholt, H. Doddapaneni, X. Qin, V. Menon, Q. Meng, G. Metcalf, H. Chao, M. C. Gingras, V. Avadhanula, P. Farinholt, C. Agrawal, D.M. Muzny, P.A. Piedra, R. A. Gibbs, J. Petrosino, Transmission event of SARS-CoV-2 delta variant reveals multiple vaccine breakthrough infections, BMC Med. 19 (2021) 255.
[5] A. Stern, S. Fleishon, T. Kustin, E. Dotan, M. Mandelboim, O. Erster, E. Mendelson, O. Mor, N.S. Zuckerman, (2021).
[6] H. Izumi, L.A. Nafie, R.K. Dukor, Conformational variability correlation prediction of transmissibility and neutralization escape ability for multiple mutation SARS-CoV-2 strains using SSSCPreds, ACS Omega 6 (29) (2021) 19323–19329.
[7] D. Planas, D. Veyer, A. Baidaliuk, I. Staropoli, F. Guivel-Benhassine, M.M. Rajah, C. Planchais, F. Porrot, N. Robillard, J. Puech, M. Prot, F. Gallais, P. Gantner, A. Velay, J. Le Guen, N. Kassis-Chikhani, D. Edriss, L. Belec, A. Seve, L. Courtellemont, H. Péré, L. Hocqueloux, S. Fafi-Kremer, T. Prazuck, H. Mouquet, T. Bruel, E. Simon-Lorière, F.A. Rey, O. Schwartz, Reduced sensitivity of SARS-CoV-2 variant delta to antibody neutralization, Nature 596 (7871) (2021) 276–280.
[8] E. Cho, M. Rosa, R. Anjum, S. Mehmood, M. Soban, M. Mujtaba, K. Bux, S.T. Moin, M. Tanweer, S. Dantu, A. Pandini, J. Yin, H. Ma, A. Ramanathan, B. Islam, A. Mey, D. Bhowmik, S. Haider, Dynamic Profiling of beta-coronavirus 3CL M(pro) protease ligand-binding sites, J. Chem. Inf. Model. 61 (2021) 3058–3073.
[9] L. Zhang, D. Lin, X. Sun, U. Curth, C. Drosten, L. Sauerhering, S. Becker, K. Rox, R. Hilgenfeld, Crystal structure of SARS-CoV-2 main protease provides a basis for design of improved alpha-ketoamide inhibitors, Science 368 (2020) 409–412.
[10] M.H. Baig, T. Sharma, I. Ahmad, M. Abohashrh, M.M. Alam, J.-J. Dong, Is PF-00835231 a pan-SARS-CoV-2 Mpro inhibitor? a comparative study, Molecules 26 (6) (2021) 1678.
[11] J. Qiao, Y.-S. Li, R. Zeng, F.-L. Liu, R.-H. Luo, C. Huang, Y.-F. Wang, J. Zhang, B. Quan, C. Shen, X. Mao, X. Liu, W. Sun, W. Yang, X. Ni, K. Wang, L. Xu, Z.-L. Duan, Q.-C. Zou, H.-L. Zhang, W. Qu, Y.-H.-P. Long, M.-H. Li, R.-C. Yang, X. Liu, J. You, Y. Zhou, R. Yao, W.-P. Li, J.-M. Liu, P. Chen, Y. Liu, G.-F. Lin, X. Yang, J. Zou, L. Li, Y. Hu, G.-W. Lu, W.-M. Li, Y.-Q. Wei, Y.-T. Zheng, J. Lei, S. Yang, SARS-CoV-2 M(pro) inhibitors with antiviral activity in a transgenic mouse model, Science 371 (6536) (2021) 1374–1378.
[12] E.J. Niesor, G. Boivin, E. Rhéaume, R. Shi, V. Lavoie, N. Goyette, M.-E. Picard, A. Perez, F. Laghrissi-Thode, J.-C. Tardif, Inhibition of the 3CL protease and SARS-CoV-2 replication by dalcetrapib, ACS Omega 6 (25) (2021) 16584–16591.
[13] H.T.H. Chan, M.A. Moesser, R.K. Walters, T.R. Malla, R.M. Twidale, T. John, H. M. Deeks, T. Johnston-Wood, V. Mikhailov, R.B. Sessions, W. Dawson, E. Salah, P. Lukacik, C. Strain-Damerell, C.D. Owen, T. Nakajima, K. Świderek, A. Lodola, V. Moliner, D.R. Glowacki, J. Spencer, M.A. Walsh, C.J. Schofield, L. Genovese, D. K. Shoemark, A.J. Mulholland, F. Duarte, G.M. Morris, Discovery of SARS-CoV-2 M(pro) peptide inhibitors from modelling substrate and ligand binding, Chem. Sci. 12 (41) (2021) 13686–13703.
[14] J.R.A. Silva, H.G. Kruger, F.A. Molfetta, Drug repurposing and computational modeling for discovery of inhibitors of the main protease (Mpro) of SARS-CoV-2, RSC Adv. 11 (38) (2021) 23450–23458.
[15] A. Citarella, A. Scala, A. Piperno, N. Micale, SARS-CoV-2 M(pro): a potential target for peptidomimetics and small-molecule inhibitors, Biomolecules 11 (4) (2021) 607.
[16] J. Yang, X. Lin, N. Xing, Z. Zhang, H. Zhang, H. Wu, W. Xue, Structure-based discovery of novel nonpeptide inhibitors targeting SARS-CoV-2 M(pro), J. Chem. Inf. Model. 61 (2021) 3917–3926.
[17] D. Sharma, A. Kunamneni, Recent progress in the repurposing of drugs/molecules for the management of COVID-19, Expert. Rev. Anti. Infect. Ther. 19 (2021) 889–897.
[18] M.P. Christy, Y. Uekusa, L. Gerwick, W.H. Gerwick, Natural products with potential to treat RNA virus pathogens including SARS-CoV-2, J. Nat. Prod. 84 (2021) 161–182.
[19] H. Yang, J. Yang, A review of the latest research on M(pro) targeting SARS-COV inhibitors, RSC Med. Chem. 12 (2021) 1026–1036.
[20] N. Drayman, J.K. DeMarco, K.A. Jones, S.-A. Azizi, H.M. Froggatt, K. Tan, N. I. Maltseva, S. Chen, V. Nicolaescu, S. Dvorkin, K. Furlong, R.S. Kathayat, M. R. Firpo, V. Mastrodomenico, E.A. Bruce, M.M. Schmidt, R. Jedrzejczak, M.Á. Muñoz-Alía, B. Schuster, V. Nair, K.-Y. Han, A. O'Brien, A. Tomatsidou, B. Meyer, M. Vignuzzi, D. Missiakas, J.W. Botten, C.B. Brooke, H. Lee, S.C. Baker, B.C. Mounce, N.S. Heaton, W.E. Severson, K.E. Palmer, B.C. Dickinson, A. Joachimiak, G. Randall, S. Tay, Masitinib is a broad coronavirus 3CL inhibitor that blocks replication of SARS-CoV-2, Science 373 (6557) (2021) 931–936.
[21] K. Gao, R. Wang, J. Chen, J.J. Tepe, F. Huang, G.W. Wei, Perspectives on SARS-CoV-2 main protease inhibitors, J. Med. Chem. 64 (2021) 16922–16955.
[22] D.R. Owen, C.M.N. Allerton, A.S. Anderson, L. Aschenbrenner, M. Avery, S. Berritt, B. Boras, R.D. Cardin, A. Carlo, K.J. Coffman, A. Dantonio, L.i. Di, H. Eng, R. A. Ferre, K.S. Gajiwala, S.A. Gibson, S.E. Greasley, B.L. Hurst, E.P. Kadar, A. S. Kalgutkar, J.C. Lee, J. Lee, W. Liu, S.W. Mason, S. Noell, J.J. Novak, R.S. Obach, K. Ogilvie, N.C. Patel, M. Pettersson, D.K. Rai, M.R. Reese, M.F. Sammons, J. G. Sathish, R.S.P. Singh, C.M. Steppan, A.E. Stewart, J.B. Tuttle, L. Updyke, P. R. Verhoest, L. Wei, Q. Yang, Y. Zhu, An oral SARS-CoV-2 Mpro inhibitor clinical candidate for the treatment of COVID-19, Science 374 (6575) (2021) 1586–1593.
[23] T. Wang, K. Xu, L. Zhao, R. Tong, L. Xiong, J. Shi, Recent research and development of NDM-1 inhibitors, Eur. J. Med. Chem. 223 (2021), 113667.
[24] J. Lee, L.J. Worrall, M. Vuckovic, F.I. Rosell, F. Gentile, A.T. Ton, N.A. Caveney, F. Ban, A. Cherkasov, M. Paetzel, N.C.J. Strynadka, Crystallographic structure of wild-type SARS-CoV-2 main protease acyl-enzyme intermediate with physiological C-terminal autoprocessing site, Nat. Commun. 11 (2020) 5877.
[25] Z. Jin, X. Du, Y. Xu, Y. Deng, M. Liu, Y. Zhao, B. Zhang, X. Li, L. Zhang, C. Peng, Y. Duan, J. Yu, L. Wang, K. Yang, F. Liu, R. Jiang, X. Yang, T. You, X. Liu, X. Yang, F. Bai, H. Liu, X. Liu, L.W. Guddat, W. Xu, G. Xiao, C. Qin, Z. Shi, H. Jiang, Z. Rao, H. Yang, Structure of M(pro) from SARS-CoV-2 and discovery of its inhibitors, Nature 582 (2020) 289–293.
[26] J.-Z. Chigan, J.-Q. Li, H.-H. Ding, Y.-S. Xu, L.u. Liu, C. Chen, K.-W. Yang, Hydroxamates as a potent skeleton for the development of metallo-β-lactamase inhibitors, Chem. Biol. Drug Des. 99 (2) (2022) 362–372, https://doi.org/10.1111/cbdd.13990.
[27] J.Q. Li, L.Y. Sun, Z.H. Jiang, C. Chen, H. Gao, J.Z. Chigan, H.H. Ding, K.W. Yang, Diaryl-substituted thiosemicarbazone: A potent scaffold for the development of New Delhi metallo-β-lactamase-1 inhibitors, Bioorg. Chem. 107 (2021), 104576.
[28] H.A. Alhadrami, A.M. Hassan, R. Chinnappan, H. Al-Hadrami, W.H. Abdulaal, E. I. Azhar, M. Zourob, Peptide substrate screening for the diagnosis of SARS-CoV-2 using fluorescence resonance energy transfer (FRET) assay, Mikrochim. Acta 188 (2021) 137.
[29] L.Y. Sun, C. Chen, J. Su, J.Q. Li, Z. Jiang, H. Gao, J.Z. Chigan, H.H. Ding, L. Zhai, K. W. Yang, Ebsulfur and Ebselen as highly potent scaffolds for the development of potential SARS-CoV-2 antivirals, Bioorg. Chem. 112 (2021), 104889.
[30] S. Iketani, F. Forouhar, H. Liu, S.J. Hong, F.Y. Lin, M.S. Nair, A. Zask, Y. Huang, L. Xing, B.R. Stockwell, A. Chavez, D.D. Ho, Lead compounds for the development of SARS-CoV-2 3CL protease inhibitors, Nat. Commun. 12 (2021) 2016.
[31] Y. Liu, C. Chen, L.Y. Sun, H. Gao, J.B. Zhen, K.W. Yang, meta-Substituted benzenesulfonamide: a potent scaffold for the development of metallo-beta-lactamase ImiS inhibitors, RSC Med. Chem. 11 (2020) 259–267.
[32] B. Atasever Arslan, B. Kaya, O. Sahin, S. Baday, C.C. Saylan, B. Ulkuseven, The iron (III) and nickel(II) complexes with tetradentate thiosemicarbazones. Synthesis, experimental, theoretical characterization, and antiviral effect against SARS-CoV-2, J. Mol. Struct. 1246 (2021), 131166.
[33] C. Ma, M.D. Sacco, B. Hurst, J.A. Townsend, Y. Hu, T. Szeto, X. Zhang, B. Tarbet, M.T. Marty, Y. Chen, J. Wang, Boceprevir, GC-376, and calpain inhibitors II, XII inhibit SARS-CoV-2 viral replication by targeting the viral main protease, Cell Res. 30 (2020) 678–692.
[34] J.Q. Li, C. Chen, M. Yao, L.Y. Sun, H. Gao, J. Chigan, K.W. Yang, Hydroxamic acid with benzenesulfonamide: An effective scaffold for the development of broad-spectrum metallo-beta-lactamase inhibitors, Bioorg. Chem. 105 (2020), 104436.
[35] D. Ghazanfari, M.S. Noori, S.C. Bergmeier, J.V. Hines, K.D. McCall, D.J. Goetz, A novel GSK-3 inhibitor binds to GSK-3beta via a reversible, time and Cys-199-dependent mechanism, Bioorg. Med. Chem. 40 (2021), 116179.
[36] E.N. Parker, J. Song, G.D. Kishore Kumar, S.O. Odutola, G.E. Chavarria, A. K. Charlton-Sevcik, T.E. Strecker, A.L. Barnes, D.R. Sudhan, T.R. Wittenborn, D. W. Siemann, M.R. Horsman, D.J. Chaplin, M.L. Trawick, K.G. Pinney, Synthesis and biochemical evaluation of benzoylbenzophenone thiosemicarbazone

analogues as potent and selective inhibitors of cathepsin L, Bioorg. Med. Chem. 23 (21) (2015) 6974–6992.
[37] J.M. Strelow, A perspective on the kinetics of covalent and irreversible inhibition, SLAS Discov. 22 (1) (2017) 3–20.
[38] C. Chen, L.Y. Sun, H. Gao, P.W. Kang, J.Q. Li, J.B. Zhen, K.W. Yang, Identification of cisplatin and palladium(II) complexes as potent metallo-beta-lactamase inhibitors for targeting carbapenem-resistant enterobacteriaceae, ACS Infect. Dis. 6 (2020) 975–985.
[39] Y. Ge, L.W. Xu, Y. Liu, L.Y. Sun, H. Gao, J.Q. Li, K. Yang, Dithiocarbamate as a valuable scaffold for the inhibition of metallo-beta-lactmases, Biomolecules 9 (2019).
[40] D. Sviben, B. Bertoša, A. Hloušek-Kasun, D. Forcic, B. Halassy, M. Brgles, Investigation of the thermal shift assay and its power to predict protein and virus stabilizing conditions, J. Pharm. Biomed. Anal. 161 (2018) 73–82.
[41] R.P. Bhusal, K. Patel, B.X.C. Kwai, A. Swartjes, G. Bashiri, J. Reynisson, J. Sperry, I. K.H. Leung, Development of NMR and thermal shift assays for the evaluation of Mycobacterium tuberculosis isocitrate lyase inhibitors, Medchemcomm 8 (11) (2017) 2155–2163.
[42] C. Ma, Y. Hu, J.A. Townsend, P.I. Lagarias, M.T. Marty, A. Kolocouris, J. Wang, Ebselen, disulfiram, carmofur, PX-12, tideglusib, and shikonin are nonspecific promiscuous SARS-CoV-2 Main protease inhibitors, ACS Pharmacol. Transl. Sci. 3 (6) (2020) 1265–1277.
[43] G.G. Rossetti, M. Ossorio, S. Barriot, L. Tropia, V.S. Dionellis, C. Gorgulla, H. Arthanari, P. Mohr, R. Gamboni, T.D. Halazonetis, (2020).
[44] N.M. Tam, P.C. Nam, D.T. Quang, N.T. Tung, V.V. Vu, S.T. Ngo, Binding of inhibitors to the monomeric and dimeric SARS-CoV-2 Mpro, Rsc Adv. 11 (5) (2021) 2926–2934.
[45] T.R. Malla, A. Tumber, T. John, L. Brewitz, C. Strain-Damerell, C.D. Owen, P. Lukacik, H.T.H. Chan, P. Maheswaran, E. Salah, F. Duarte, H. Yang, Z. Rao, M. A. Walsh, C.J. Schofield, Mass spectrometry reveals potential of beta-lactams as SARS-CoV-2 M(pro) inhibitors, Chem. Commun. (Camb.) 57 (2021) 1430–1433.
[46] P.W. Thomas, M. Cammarata, J.S. Brodbelt, A.F. Monzingo, R.F. Pratt, W. Fast, A Lysine-Targeted Affinity Label for Serine-beta-Lactamase Also Covalently Modifies New Delhi Metallo-beta-lactamase-1 (NDM-1), Biochemistry 58(25) (2019) 2834-2843.
[47] S.O. Aftab, M.Z. Ghouri, M.U. Masood, Z. Haider, Z. Khan, A. Ahmad, N. Munawar, Analysis of SARS-CoV-2 RNA-dependent RNA polymerase as a potential therapeutic drug target using a computational approach, J Transl Med, 18 (2020) 275.
[48] H.-H. Ding, M.-H. Zhao, L.e. Zhai, J.-B. Zhen, L.-Y. Sun, J.-Z. Chigan, C. Chen, J.-Q. Li, H. Gao, K.-W. Yang, A quinine-based quaternized polymer: a potent scaffold with bactericidal properties without resistance dagger, Polym. Chem. 12 (16) (2021) 2397–2403.
[49] L.H. Al-Wahaibi, A. Mostafa, Y.A. Mostafa, O.F. Abou-Ghadir, A.H. Abdelazeem, A. M. Gouda, O. Kutkat, N.M. Abo Shama, M. Shehata, H.A.M. Gomaa, M. H. Abdelrahman, F.A.M. Mohamed, X. Gu, M.A. Ali, L. Trembleau, B.G.M. Youssif, Discovery of novel oxazole-based macrocycles as anti-coronaviral agents targeting SARS-CoV-2 main protease, Bioorg. Chem. 116 (2021) 105363.
[50] J.S. Strobl, M. Nikkhah, M. Agah, Actions of the anti-cancer drug suberoylanilide hydroxamic acid (SAHA) on human breast cancer cytoarchitecture in silicon microstructures, Biomaterials 31 (27) (2010) 7043–7050.
[51] B.R. You, B.R. Han, W.H. Park, Suberoylanilide hydroxamic acid increases anti-cancer effect of tumor necrosis factor-α through up-regulation of TNF receptor 1 in lung cancer cells, Oncotarget 8 (11) (2017) 17726–17737.
[52] S.N. Maqbool, S.C. Lim, K.C. Park, R. Hanif, D.R. Richardson, P.J. Jansson, Z. Kovacevic, Overcoming tamoxifen resistance in oestrogen receptor-positive breast cancer using the novel thiosemicarbazone anti-cancer agent, DpC, Br. J. Pharmacol. 177 (2020) 2365–2380.
[53] B.Z. Sibuh, P.K. Gupta, P. Taneja, S. Khanna, P. Sarkar, S. Pachisia, A.A. Khan, N. K. Jha, K. Dua, S.K. Singh, S. Pandey, P. Slama, K.K. Kesari, S. Roychoudhury, Synthesis, in silico study, and anti-cancer activity of thiosemicarbazone derivatives, Biomedicines 9 (10) (2021) 1375.
[54] C. Chen, K.-W. Yang, L.e. Zhai, H.-H. Ding, J.-Z. Chigan, Dithiocarbamates combined with copper for revitalizing meropenem efficacy against NDM-1-producing Carbapenem-resistant Enterobacteriaceae, Bioorg. Chem. 118 (2022) 105474.
[55] J. Li, W. Yang, W. Zhou, C. Li, Z. Cheng, M. Li, L. Xie, Y. Li, Aggregation-induced emission in fluorophores containing a hydrazone structure and a central sulfone: restricted molecular rotation, Rsc Adv. 6 (42) (2016) 35833–35841.